JOURNAL OF SOLID STATE CHEMISTRY 4, 163–171 (1972)

Hall Effect, Magnetoresistance, and Thermoelectric Power in Lithium Tetraammine*

E. W. LEMASTER† AND J. C. THOMPSON

Department of Physics, The University of Texas at Austin, Austin, Texas 78712

Received December 11, 1970

Data are reported here on the Hall coefficient of polycrystalline $Li(NH_3)_4$ from 1.5 to 89 K, the thermoelectric power from 4.2 to 89 K (and on into the melt), and the transverse magnetoresistance at several temperatures in the range 1.5 to 77 K.

In the fcc phase ($82 \leqslant T \leqslant 89$ K) where there is one Li atom per primitive cell, the Hall coefficient is negative and approximately equal to the free-electron value, and the thermoelectric power is positive.

In the hexagonal phase ($T \leqslant 82$ K) there are two Li atoms per primitive cell. The Hall coefficient is negative and shows little change with temperature down to about 10 K where it becomes less negative. The thermoelectric power is negative down to 26 K where it becomes positive. By fitting the data to a two-band compensated model ($n_e = n_h$) it is found that the number densities of charge carriers vary with temperature at $T \leqslant 47$ K. It is thus concluded that the model is too simple for the low-temperature behavior of $Li(NH_3)_4$.

I. Introduction

Lithium tetraammine, $Li(NH_3)_4$, is one of a class of metallic compounds formed between ammonia and alkali or alkaline-earth metals (*1*). Its low-temperature transport properties (*2–9*) are much like those of a compensated metal, such as tungsten. At low temperatures the crystal structure is hexagonal and there is a first-order phase transition to fcc at 82 K, only 7 K below the melting point (*10–12*).

We report here data on the Hall coefficient and thermoelectric power (TEP) from 4.2 to 89 K. Also included are new data on the transverse magnetoresistance (MR) at several temperatures in the range 1.5 to 77 K. Previous measurements of the Hall coefficient were taken by Jaffe (*2*) at only two temperatures, 83 and 58 K. The double-ac technique used here for measuring the Hall coefficient makes it possible to take data continuously as the sample warms from helium temperatures. From the present data and the resistivity, electron and hole mobilities and number densities are calculated on a two-band model.

* Work supported by the National Science Foundation and The Robert A. Welch Foundation.

† Present address: Physical Science Department, Pan American College, Edinburg, TX 78539.

II. Experimental

Sample preparation. All samples were contained in Pyrex cells with electropolished tungsten electrodes. Samples were prepared as stoichiometric liquids in the following manner: Lithium of at least 99.9% purity was cut, weighed, and placed in a metal dropper while in the dry helium atmosphere of a glove box. The metal dropper was placed above the mixing vessel containing a glass-enclosed magnet stirrer. The whole assembly was evacuated, the metal dropper closed off, and the mixing vessel and sample cell were rinsed with dried ammonia. After removal of the liquid ammonia, the metal was dropped into the mixing vessel, ammonia added, and the solution was then mixed and poured into the sample cell. The solution was finally frozen in liquid N_2 and sealed off under vacuum.

The details of the sample cell design are shown in Fig. 1. Figure 1(a) shows the current electrodes A and B, the Hall voltage electrodes C and D, and the conductivity electrodes D and E. Note that the length to width ratio is in excess of 4:1 (*13*). The thermopower cell of Fig. 1(b) has four electrodes: H and I for the potential difference measurement and F and G for improving thermal contact between the sample, bath, and thermometer (G).

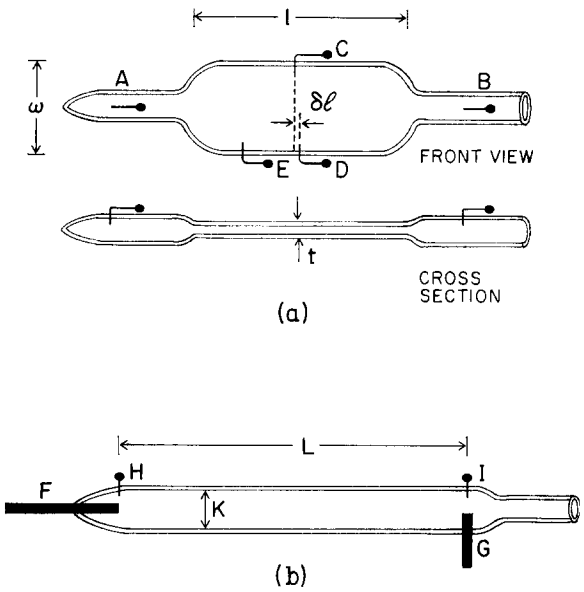

FIG. 1. (a) The Hall cell is made of Pyrex plates of dimensions: $l = 50$ mm, $w = 9$ mm, and $t = 0.635$ mm. The current electrodes, A and B, are 25 mil tungsten; the Hall electrodes, C and D, and the conductivity electrode, E, are 15 mil tungsten. Silver solder beads are on all electrodes so that Pb solder can be used to connect wiring to the electrodes. (b) The thermoelectric power cell is made of Pyrex tubing having dimensions $K = 8$ mm, and $L = 20$ cm. The tungsten electrodes, F and G, are 150 mil and electrodes H and I are 25 mil.

On the basis of previous observations (*2–6*), all samples were either solidified slowly in a temperature gradient from the bottom up, or zone refined to insure a continuous, void-free sample. The transverse magnetoresistance at 15 kG and 4.2 K was recorded for several samples as a function of rotation angle about the axis of the sample. There was less than 5% anisotropy. It was thus concluded that the samples were polycrystalline. There are several reasons for the polycrystallinity: (1) The crystal structure change at 82 K is first-order and accompanied by a volume change of about 2%. (2) There is adhesion between the sample and Pyrex container and most likely a difference in expansion rates. (3) An anomaly in the resistivity exists at about 65 K (*4–5*) which may be due to (1) and (2), or it may be a Martensitic transition (X-ray data (*11, 12*) exist only above 77 K).

Measurements. The double-ac method of measuring the Hall coefficient was developed by Russell and Whalig (*14*) and described in detail by Nasby (*15*). The temperature was varied from the freezing point of the solution at 89 to 50 K by pumping on liquid nitrogen. At lower temperatures the data were taken as the sample warmed from 4.2 K at a rate of about 1 K/min, depending on the current and magnetic field being used. The temperature was measured in the liquid nitrogen range with a copper–constantan thermocouple and with a calibrated carbon resistor in the low-temperature range.

The ac magnet gave a maximum zero-to-peak field of 3 kG in the center of the 2-in. gap of the 6-in. square laminated poles. For measuring the ac–dc Hall Effect and magnetoresistance the same magnet was operated on dc to give a maximum field of 3 kG measured with a rotating coil gaussmeter. The ac–dc Hall method involved the use of a bucking circuit to suppress the misalignment voltage from the Hall electrodes, C and D in Fig. 1(a). The transverse signal was measured with a lock-in amplifier for the forward and reverse directions of the magnetic field. The two deflections thus obtained were subtracted to yield twice the Hall voltage. By averaging the two signals, one can obtain the "transverse-even" voltage which generally has the same behavior as the transverse magnetoresistance in polycrystalline samples. The magnetoresistance was measured from electrodes D and E in Fig. 1(a) using a standard 4-probe technique.

The thermoelectric power was measured against Pb using the integral method (*16*). The lower electrodes, F and H in Fig. 1(b), were immersed in liquid nitrogen or liquid helium while the top end of the sample was warmed with a bifilar heater above electrodes G and I. The temperature at electrode G was measured with the thermocouple and resistor in good contact with G. The Seebeck voltage versus temperature was plotted on large graph paper and the slope determined graphically.

III. Data

Resistivity. Jaffe (*2*) observed a nonreproducible resistivity below 83 K which he attributed to "cracks and fissures" in the sample material. Similar effects were also observed in this work in the temperature range 60–70 K even though great care was taken to anneal the material above and below the structure change at 82 K (*17*). Sample cells with different surface-to-volume ratios were used so that sample-container effects could be investigated. The resistivity increase below 20 K was independent of the container. The sluggishness of the resistivity changes with respect to temperature and the absence of a latent heat (*10*) suggests that the behavior of the resistance is due to a Martensitic transition. Perhaps the transition involves the symmetry of the stacking of the $Li–NH_3$ tetrahedra (*12*). The Martensitic

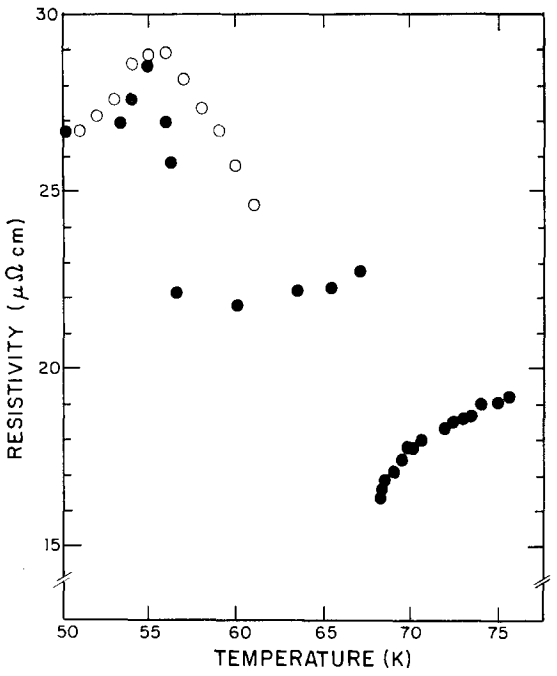

FIG. 2. The electrical resistivity in the region of the resistivity jump shown in the inset of Fig. 3. These data were taken with a four-probe method. The solid circles show data taken as the sample cooled; the open circles were taken as the sample warmed.

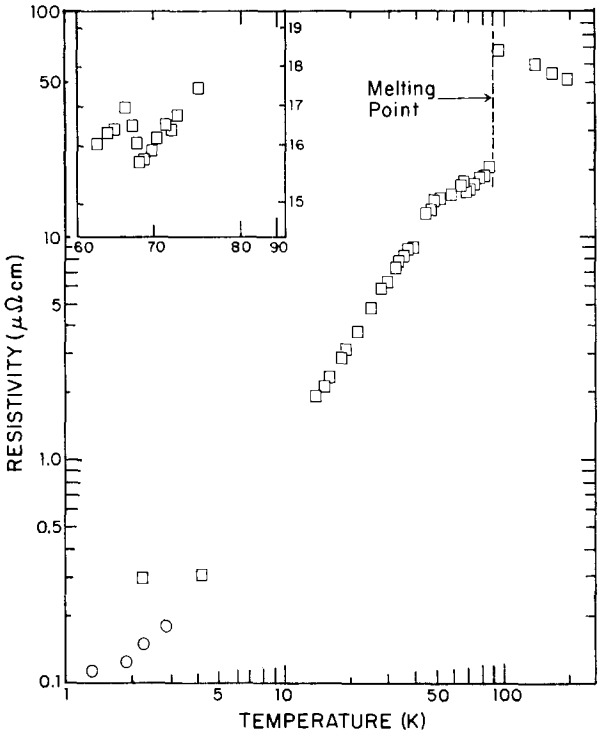

FIG. 3. The resistivity versus temperature of $Li(NH_3)_4$ measured with an electrodeless method. The data of McDonald and Thompson (*5*) are shown as squares and the circles are the data of Cate and Thompson (*6*). The vertical dashed line shows the melting point and there is a jump in the resistivity at the solid–solid phase transition at 82.2 K. The inset shows a resistivity jump at 67 K also.

transition in pure Li at about 78 K (*18*) from bcc to hcp is probably not related (*7*). Figure 2 shows the resistivity in the temperature range concerned. The large increase in resistivity below 55 K is anomalous; it indicates that the effect(s) taking place at 60–70 K probably cause strains.

Since the four-probe resistivity data collected in this study show erratic behavior below 70 K, we present here, and subsequently use, resistivity data of McDonald (*5*) and Cate (*6*). Their electrodeless technique was not extremely sensitive to the continuity of the sample; however, voids or very small crystallites would have the effect of increasing the apparent resistivity. Figure 3 shows the electrodeless resistivity data over the temperature range 1.5–200 K. The vertical dashed line indicates the freezing point of the solution at 89 K. There is a slight change visible at the phase change at 82 K, but on this scale the change at 67 K doesn't appear. Also to be noted is the fact that the electrodeless data show no large increase below 67 K as is seen in the four-probe data. As Morgan (*19*) has pointed out, the temperature variation fits a Bloch–Gruneisen equation over the temperature range 15–80 K with a Debye temperature of 55 K. The low-temperature behavior can be fitted by an equation of the form (*6*) $\rho = AT^2 + BT^5$. The T^5 component is the normal low-temperature electron–phonon interaction, and the T^2 dependence is similar to that observed in polycrystalline ^{20}Bi, In, and ^{21}Al and attributed to electron–electron interactions (*6*) among other possibilities.

Magnetoresistance (MR). The MR of polycrystalline $Li(NH_3)_4$ is shown in Fig. 4. The data may be fit to a straight line of slope 1.4; this indicates that the MR obeys a power law of the form

$$[\rho(B) - \rho(0)]/\rho(0) = \Delta\rho/\rho = |\mathbf{B}|^m, \quad \begin{cases} m = 1.4, & B > 1 \text{ kG}; \\ m = 1, & B < 1 \text{ kG}. \end{cases} \quad (1)$$

The linear behavior for fields below 1 kG, indicated in Eq. (1), is shown in Fig. 5 at 4.2 K. The change in power law near 1 kG was also seen in electrodeless MR studies by Cate (*6*). The exponent above 1 kG has been observed (*5*, *6*) to lie in the range $1.3 \leqslant m \leqslant 2.0$, with the preponderance of our results near 1.4. The data is presented as a logarith-

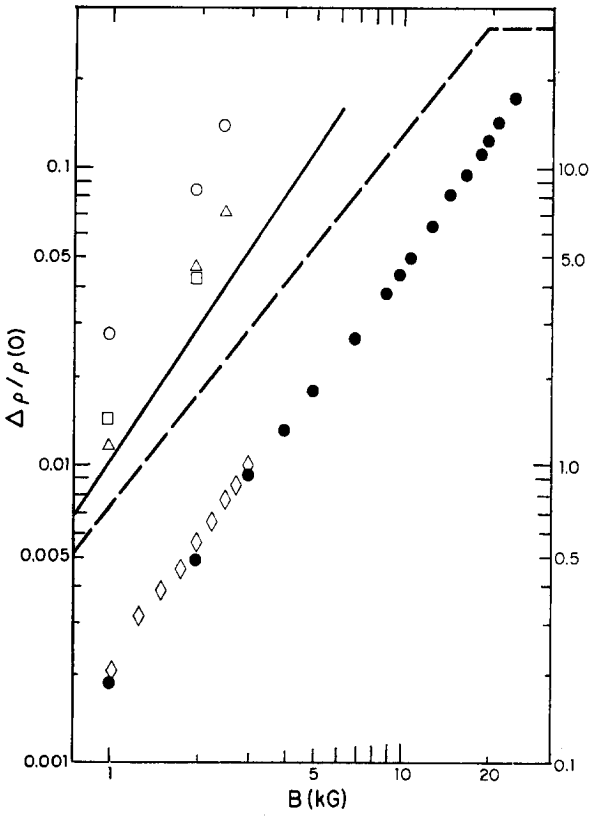

FIG. 4. The MR versus magnetic field for several samples at different temperatures; zero-field resistivities are indicated below. ● Sample II, $\rho(0) = 9$ $\mu\Omega$ cm at 4.2 K; — Jaffe (2), $\rho(0) = 400$ $\mu\Omega$ cm at 21 K; ◇ Sample IX, $\rho(0) = 10.8$ $\mu\Omega$ cm at 4.2 K; △ Sample IX, $\rho(0) = 13.3$ $\mu\Omega$ cm at $T = 47.5$ K; □ Sample IX, $\rho(0) = 10.9$ $\mu\Omega$ cm at 62 K; ○ Sample IX, $\rho(0) = 11$ $\mu\Omega$ cm at 77.5 K. Note that (●) Sample II and (◇) Sample IX refer to the right-hand scale.

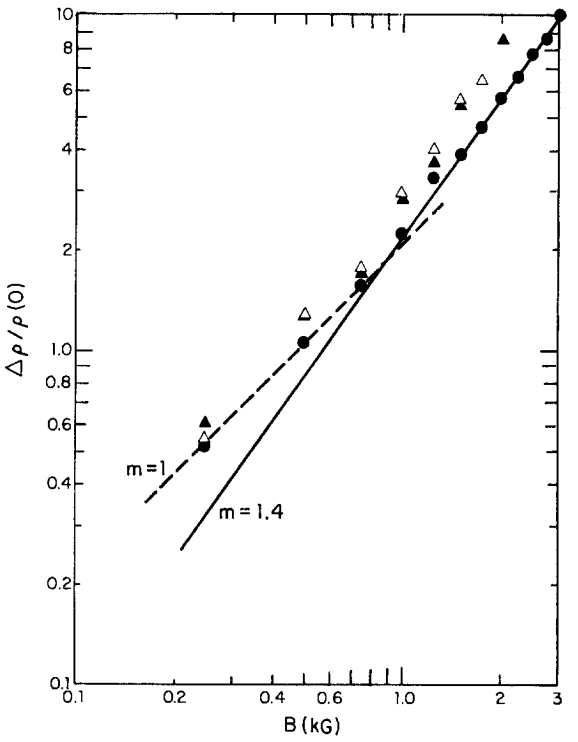

FIG. 5. The MR in low magnetic fields which shows the linear dependence on field below 1 kG. The data are all presented for Sample IX, ⊥ designates a sample oriented with the plane of the Hall cell perpendicular to the field, and ∥ is parallel to the field. △, $\rho(0) = 10$ $\mu\Omega$ cm at 1.46 K, ⊥; ▲, $\rho(0) = 10$ $\mu\Omega$ cm at 1.46 K, ∥; ●, 10.8 $\mu\Omega$ cm = $\rho(0)$ at 4.2 K, ⊥. The slopes of the straight lines are indicated by the values of m.

mic plot to show the field dependence of the MR; the magnitude is not reliable because of the 4-probe resistivity problems mentioned above.

Hall Effect. The Hall data are presented in terms of the reduced Hall coefficient, R_H/R_{FE}, where R_H is the experimental value and R_{FE} is the free electron value calculated from the mass density at 77 K with the assumption of one free electron contributed by each Li atom, $R_{FE} = 1/nec = -1.37 \times 10^{-3}$ cm^3/C.

In measuring the Hall voltage, one observes a zero field signal on the transverse electrodes due to misalignment of the electrodes. The transverse voltage can be expressed in terms of the misalignment δl, the cross-sectional area of the cell A, and the resistivity of the sample, ρ. This expression is

$$V_Y = V_H + i(\omega_1) r = V_H + i(\omega_1)\rho\delta l/A, \quad (2)$$

where the Hall voltage is related to the Hall coefficient by $V_H = R_H i(\omega_1) B(\omega_2)/\tau$ and the thickness of the Hall cell is τ. The current and magnetic field frequencies are indicated by ω_1 and ω_2, respectively. The second term on the right-hand side of Eq. (2) is the misalignment voltage, $V_b = i(\omega_1)\rho\delta l/A$, which can be suppressed with a bucking voltage of frequency ω_1. This technique is adequate until the resistivity shows appreciable dependence on magnetic field. Then the second term depends on both the current frequency and the magnetic-field frequency just as the Hall voltage. Because of this behavior, the double-ac Hall technique yields erroneous results for the Hall voltage.

One may extract the "true" Hall voltage from the double-ac data as follows. The MR is responsible for the spurious signal at the same frequency as the Hall signal and, since the MR shows two different power law dependences, the problem must be considered for each region. These are written

$$\begin{aligned} \Delta\rho/\rho &= C_1|\mathbf{B}(\omega_2)|, \quad B < 1 \text{ kG}; \\ \Delta\rho/\rho &= C_2|\mathbf{B}(\omega_2)|^{1.4}, \; B > 1 \text{ kG}; \end{aligned} \quad (3)$$

where $|\mathbf{B}(\omega_2)|$ indicates that the MR depends only on the modulus of the time-dependent magnetic field.

1. $B < 1$ *kG*. If we write the expression for the signal appearing on the Hall electrodes in this range of magnetic field, we find from Eq. (2)

$$V_Y = V_H + i(\omega_1)\rho(0)\,\delta l/A + i(\omega_1)\rho(0)\,C_1|\mathbf{B}(\omega_2)|\,\delta l/A. \quad (4a)$$

The second term on the right is V_b and can be suppressed as before. The last term has large contributions at the frequencies of the Hall signal, $\omega_1 \pm \omega_2$, as well as higher harmonics. One can obtain the true Hall voltage below 1 kG by experimentally determining the quantities in the last term of Eq. (4a) and expanding $|\mathbf{B}(\omega_2)| = \mathbf{B}_0|\cos\omega_2 t|$ in a Fourier series to find the amount of contribution at the frequency ω_2. Because the data above 1 kG showed less relative error, the actual procedure was to obtain the true Hall voltage from the data above 1 kG using a procedure we next describe.

2. $B > 1$ *kG*. The expression for the transverse signal V_Y is

$$V_Y = V_H + i(\omega_1)\rho(0)\,\delta l/A + i(\omega_1)\rho(0)\,C_2|B(\omega_2)|^{1.4}\,\delta l/A. \quad (4b)$$

The second term on the right is again V_b. In the last term there is a factor $|B(\omega_2)|^{1.4} = B_0^{1.4}|\cos\omega_2 t|^{1.4}$ and current can be written $i(\omega_1) = I_0\cos w_1 t$. Substituting into Eq. (4b), we find

$$V_Y = V_H + V_b + [\rho(0)\,\delta l I_0 B_0^{1.4} \times \cos\omega_1 t|\cos\omega_2 t|/A]\,|\cos\omega_2 t|^{0.4}, \quad (5)$$

or

$$V_Y = V_H + V_b + G|\cos\omega_2 t|^{0.4}, \quad (6)$$

where $G = [\rho(0)\delta l I_0 B_0^{1.4}\cos\omega_1 t|\cos\omega_2 t|/A]$ contains terms of frequency $\omega_1 \pm \omega_2$, the same as the Hall signal. The fractional-power cosine term in the last term of Eq. (6) can be expanded in a Fourier series. The constant term a_0 in such an expansion then gives a term on the right-hand side of Eq. (6), $a_0 G$, which has a frequency dependence the same as the Hall voltage, as well as higher harmonics. The difference between the field dependence of the Hall voltage and the $a_0 G$ term gives a clue to obtaining the true Hall voltage. Let us write from Eq. (6) the terms having the frequency dependence of the Hall signal

$$V_Y\tau/I_0 B_0 = (V_H\tau/I_0 B_0) + (a_0 G\tau/I_0 B_0). \quad (7)$$

This can be written as

$$R_H|_{\text{err}} = R_H + a_0[\rho(0)\,\delta l B_0^{0.4}\cos\omega_1 t|\cos\omega_2 t|/A]\tau. \quad (8)$$

If R_H has no magnetic-field dependence, then the true Hall coefficient may be extracted by extrapolating the measured $R_H|_{\text{err}} = V_Y\tau/I_0 B_0$ to $B = 0$. These results have been compared in Fig. 6 with the results of an ac–dc measurement of the Hall constant. The $B^{0.4}$-dependence expected from Eq. (8) is confirmed; however, the R_H obtained by extrapolation is less than one half the value obtained from the ac–dc experiment. The source of this discrepancy probably lies in the ac–dc method—the misalignment signal due to MR can have components of the same frequency and phase as the Hall signal. Similar comparisons at higher temperatures, where MR effects were negligible, produced agreement within 5%, and V_Y linear in B.

Figure 7 contains Hall constants determined from ac–ac measurements near 1 kG. These data constitute an upper limit for the "true" Hall coefficient, because of the MR effects discussed above. In an attempt to estimate the effect of the MR at temperatures above 4 K, we have assumed Koehler's rule and computed corrections following Eq. (8); the corrected data are shown as open circles. The MR influence is significant only below 15 K. Uncer-

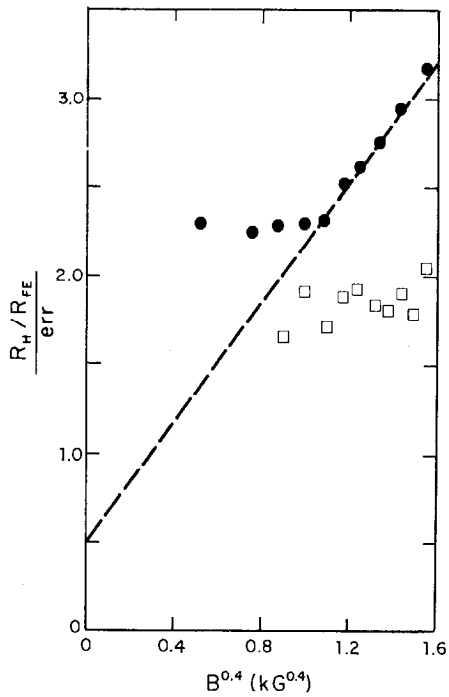

FIG. 6. The erroneous Hall coefficient as a function of the magnetic field is shown. All data are for Sample IX; the method of measuring the Hall coefficient is indicated in parentheses: ● $\rho(0) = 10.6$ $\mu\Omega$ cm at 4.2 K (ac–ac); and □ $\rho(0) = 16.9$ $\mu\Omega$ cm at 4.2 K (ac–dc). The random errors are near 20%.

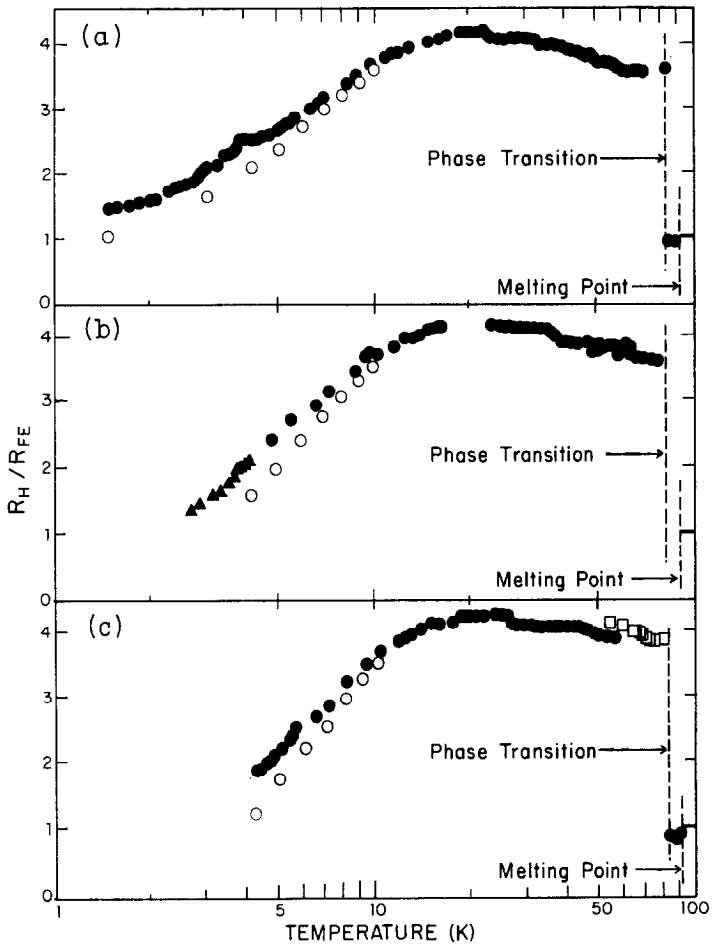

FIG. 7. The ac–ac Hall coefficient data versus temperature are shown as well as the values of the Hall coefficients extrapolated to $B = 0$. The straight line above 89 K indicates the temperature-independent Hall coefficient measured by Kyser (*23*) on a liquid sample. (a) ● Sample IX at $B = 1$ kG, and ○ extrapolated to $B = 0$. (b) ● Sample VIII at $B = 1.5$ kG, ▲ at $B = 1.0$ kG, and ○ data extrapolated to $B = 0$. (c) ● Sample VII at $B = 1.3$ kG, □ represents data taken as sample cooled from 77.5 K, and ○ shows data extrapolated to $B = 0$. The vertical dashed lines show the melting point at 89 K and the solid–solid phase transition at 82 K.

tainties over the validity of Kohler's rule (*5*, *6*) and discrepancies such as shown in Fig. 6 severely limit the accuracy of the corrections. We may nevertheless conclude that the Hall coefficient declines markedly as T is reduced below 15 K. The errors in the data in Fig. 7 are estimated to be $\pm 10\%$ above 15 K and up to 100% below. Note the large change in the Hall coefficient when the structure changes at 82 K. The data of Kyser (*23*) in the liquid has been adjusted to the density of the liquid. The data for different samples showed deviations of up to 50% below 7 K. This deviation is thought to be a result of strains induced in the sample as it was cooled quickly from 50 K by transferring liquid helium into the Dewar. A strain-dependent Hall coefficient has been seen by Krautz (*24*) in tungsten, and, in fact, a change in sign in the Hall coefficient at low temperatures appears in cold-worked tungsten.

Thermoelectric power. The absolute thermoelectric power of $Li(NH_3)_4$ is presented in Fig. 8. The data extend into the liquid region; we note for reference that the TEP of sodium–ammonia solutions (*25*) is also positive in the more concentrated solutions. There are no Li–NH_3 solution data. The other features to note are the discontinuous change in the TEP at the freezing point, the change at the phase transition at 82 K, and the gradual change in sign near 25 K.

We note that although the four-probe resistivity (Fig. 2) becomes erratic below 70 K due to sample

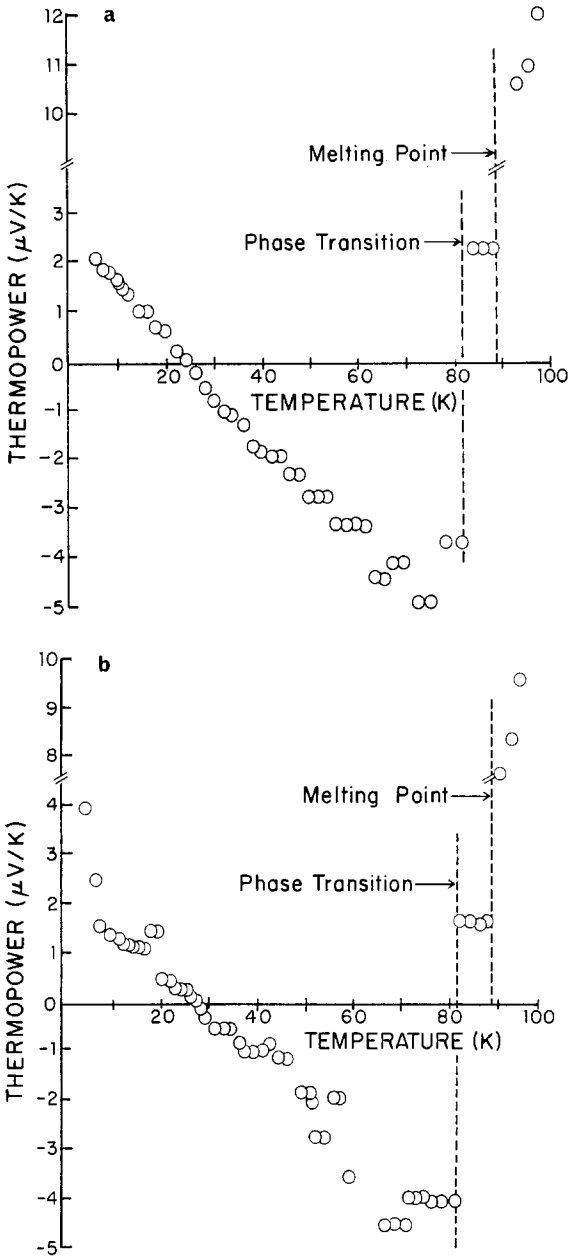

FIG. 8. (a) The thermoelectric power of a slow-frozen sample of $Li(NH_3)_4$. (b) The thermoelectric power of a zone-refined sample. Both samples were measured against Pb. Note change in ordinate.

discontinuities, these discontinuities should have little effect on the Hall and Seebeck voltages. Volger (*26*), Putley (*27*), and Herring (*28*) argue that for a model of a polycrystalline material in which there are crystallites separated by small regions of high resistivity, the measured resistivity will be considerably higher than the resistivity of the crystallites. The Hall voltage, however, will simply be an average over the orientations of the crystallites if the volume of crystallites is much greater than the material between them. The arguments would equally well apply to the Seebeck voltage. We thus believe that the data presented here on the Hall and thermoelectric effects are not sensitive to the sample effects that plagued the resistivity measurements.

IV. Discussion

The transport properties of metals are determined by the number and type of carriers available and by their interaction with the lattice. The gross properties of the electron–ion interaction can be determined from the crystal structure and whether the Fermi sphere overlaps a Brillouin zone boundary (*29*). In $Li(NH_3)_4$ there are two known crystal structures—fcc at high temperatures and hexagonal at low temperatures. In the absence of X-ray data we will assume the hexagonal structure to persist below 77 K. The properties of the metal are completely different for the two structures; so we shall discuss the available data for the two crystal structures separately.

Face-centred cubic phase, $82 \leqslant T \leqslant 89$ K. This phase contains one Li atom per primitive cell, and Li contributes one electron per atom to the conduction band. Unless the Fermi surface is highly distorted, no contact with the zone boundary is expected. This leads one to anticipate the transport properties to be in reasonable accord with the free-electron model (FEM). The Hall coefficient is in good agreement with the FEM (Fig. 7). The thermopower, however, has a positive sign as opposed to the negative sign predicted for both the diffusion and the "phonon-drag" contributions to the thermopower (*30–33*). In view of the fact that many of the alkali and noble metals have negative Hall coefficients and positive thermopowers (*34*, *35*), the behavior seen here is not surprising.

Hexagonal phase, $T \leqslant 82$ K. In this phase there are two Li atoms per primitive cell, and most probably contact between the Fermi sphere and the zone boundary. A large, nonsaturating MR as seen in $Li(NH_3)_4$ (*5*, *6*) (Fig. 4) can be caused by two-band conduction with complete compensation, by the presence of open orbits (*36*, *37*), or by a combination of the two effects. The field dependence of the MR in the two-band compensated model is proportional to B^2, while for open orbits one expects polycrystalline samples to give a near linear dependence on field (*38*). In polycrystalline samples the MR data is not easily deciphered.

The Hall coefficient for two models behaves differently as a function of magnetic field. In a two-band compensated material the Hall coefficient is expected to be independent of magnetic field. In the case of a polycrystal with open orbits possible in certain directions, one would expect to see a field-dependent R_H due to two uncompensated bands (*13*) added to the field-independent R_H resulting from open orbits (*37*). We see no field dependence in R_H up to 31 G at temperatures above 47 K. The Hall data at low temperatures is complicated by the presence of MR effects. In addition, no structural information exists below 77 K; so any model calculation must be regarded as conjecture. We have adopted, for illustration, the simplest model available.

The qualitative behavior of the Hall coefficient, high-field magnetoresistance, and conductivity can be described with a simple two-band model with complete compensation. The expressions are

$$\Delta\rho/\rho = \mu_e \mu_h B^2, \qquad \sigma = n|e|(\mu_e + \mu_h),$$
$$R_H = (nec)^{-1}(\mu_e - \mu_h)/(\mu_e + \mu_h), \tag{9}$$

where e is electron charge and c is speed of light. From these expressions we can compute the mobilities, μ_e and μ_h, and the number densities, $n_e = n_h = n$, of the electrons and holes. Table I shows the results of these calculations at several temperatures. The conductivity data is the electrodeless data shown in Fig. 3. In view of the problems with the 4-probe conductivity, the MR data reported here show only the field dependence. The electrodeless MR data of McDonald and Thompson (*5*) are thus used in the calculations along with the assumption of Kohler's rule. The large MR coefficient dominates all other terms and is responsible for the closeness of the μ_e and μ_h. The large uncertainties in R_H at low temperatures thus do not affect these calculations. The number densities are expressed as a percent of n_0, where $n_0 = 4.57 \times 10^{21}$ cm^{-3} is the number of electrons calculated from the density (*11*) of $Li(NH_3)_4$ assuming one electron per Li atom. At 47 K and below, the charge carrier densities vary with temperature which shows that the model is inadequate or that a structure charge occurs in the vicinity of 50 K. These low-charge densities, if real, require a considerable distortion of the Fermi surface by energy gaps at the zone face.

TABLE I

T (K)	μ_e (cm^2/V sec)	μ_h (cm^2/V sec)	n (cm^{-3})	n/n_0 (%)
77	0.90×10^4	0.88×10^4	2.0×10^{19}	0.44
62	0.94×10^4	0.91×10^4	2.0×10^{19}	0.44
47	1.20×10^4	1.15×10^4	2.7×10^{19}	0.59
4.2	7.15×10^4	6.45×10^4	1.1×10^{20}	2.4
1.5	12.0×10^4	10.9×10^4	2.3×10^{20}	4.9

The two-band model for the thermoelectric power shows a linear (*32*, *33*) dependence on temperature but does not predict a change in sign as is seen in the data probably because the model breaks down at lower temperatures. We note a similar behavior of the thermopower in the alkali metals (*39*) and especially in tungsten (*40*).

Further conclusions about the metallic compound $Li(NH_3)_4$ await MR data on the single crystal, X-ray data below 77 K, and Hall data at higher magnetic fields than reported here.

V. Conclusion

Lithium tetraammine shows simple free-electron behavior in the fcc structure. The positive thermopower is probably due to an energy-dependent pseudopotential.

In the hexagonal structure the behavior is best represented by a two-band compensated model. The compensation is necessary to allow for the large nonsaturating MR. By using MR, resistivity and Hall data, the electron and hole densities are found to be a small fraction of the electron density calculated from the experimental mass density. It is thus concluded that the Fermi surface is considerably distorted.

References

1. N. MAMMANO, "Proceedings of Colloque Weyl II" (J. J. Lagowski and M. J. Sienko, Eds.), p. 367, Butterworths, London, 1970.
2. H. JAFFE, *Z. Phys.* **93**, 741 (1935).
3. A. J. BIRCH AND D. K. C. MADDONALD, *Trans. Faraday Soc.* **43**, 792 (1947); **44**, 735 (1948).
4. J. A. MORGAN, R. L. SCHROEDER, AND J. C. THOMPSON, *J. Chem. Phys.* **43**, 4494 (1965).
5. W. J. MACDONALD AND J. C. THOMPSON, *Phys. Rev.* **150**, 602 (1966).
6. R. C. CATE AND J. C. THOMPSON, *J. Phys. Chem. Solids* **32**, 443 (1971).
7. R. A. LEVY, *Phys. Rev.* **102**, 31 (1956).
8. P. G. VARLASHKIN AND A. T. STEWART, *Phys. Rev.* **148**, 459 (1966); *Bull. Amer. Phys. Soc.* **11**, 167 (1966).
9. E. W. LEMASTER, *Bull. Amer. Phys. Soc.* **15**, 323 (1970).
10. N. MAMMANO AND L. V. COULTER, *J. Chem. Phys.* **47**, 564 (1967); **50**, 393 (1969).
11. N. MAMMANO AND M. J. SIENKO, *J. Amer. Chem. Soc.* **90**, 6322 (1968).
12. L. KLEINMAN, S. B. HYDER, C. M. AND J. C. THOMPSON, "Proceedings of Colloque Weyl II" (J. J. Lagowski and M. J. Sienko, Eds.), p. 229, Butterworths, London, 1970.

13. J.-P. JAN, "Solid State Physics" (F. Seitz and D. Turnbull, Eds.), Vol. 5, p. 1, Academic Press, New York, 1957.
14. B. R. RUSSELL AND C. WHALIG, *Rev. Sci. Instr.* **21**, 1028 (1950).
15. R. D. NASBY AND J. C. THOMPSON, *J. Chem. Phys.* **53**, 109 (1970).
16. G. K. WHITE, "Experimental Techniques in Low-Temperature Physics," Oxford University Press, London, 1968.
17. This procedure was suggested by M. Rosenthal.
18. C. S. BARRETT, *Acta Crystallogr.* **9**, 671 (1956).
19. J. A. MORGAN AND J. C. THOMPSON, *J. Chem. Phys.* **47**, 4607 (1967).
20. E. W. FENTON, J.-P. JAN, A. KARLSSON, AND R. SINGER, *Phys. Rev.* **184**, 663 (1969).
21. J. C. GARLAND AND R. BOWERS, *Phys. Rev. Lett.* **21**, 1007 (1968).
22. J. M. ZIMAN, "Quantum Theory of Solids," John Wiley & Sons, New York, 1967.
23. D. S. KYSER AND J. C. THOMPSON, *J. Chem. Phys.* **42**, 3910 (1965).
24. V. E. KRAUTZ AND H. SCHULTZ, *Z. Angew. Phys.* **15**, 1 (1963).
25. J. F. DEWALD AND G. LEPOUTRE, *J. Amer. Chem.* **76**, 3369 (1954); **78**, 2956 (1956).
26. J. VOLGER, *Phys. Rev.* **79**, 1023 (1950).
27. E. H. PUTLEY, "The Hall Effect and Semi-Conductor Physics," Dover, New York, 1960.
28. C. HERRING, *J. Appl. Phys.* **31**, 1939 (1960).
29. W. A. HARRISON, "Pseudopotentials in the Theory of Metals," Benjamin, New York, 1966.
30. E. H. SONDHEIMER, *Can. J. Phys.* **34**, 1246 (1956).
31. J. M. ZIMAN, "Electrons and Phonons," Clarendon Press, Oxford, 1960.
32. D. K. C. MACDONALD, "Thermoelectricity: An Introduction to the Principles," John Wiley and Sons, New York, 1962.
33. M. BAILYN, *Phil. Mag.* **5**, 1059 (1960).
34. J. E. ROBINSON AND J. D. DOW, *Phys. Rev.* **171**, 815 (1968).
35. A. MEYER AND W. H. YOUNG, *Phys. Rev.* **184**, 1003 (1969).
36. I. M. LIFSHITZ, M. YA. AZBEL, AND M. I. KAGANOV, *Zh. Eksp. Teor. Fiz.* **31**, 63 (1956); translation: *Sov. Phys. JETP* **4**, 41 (1957).
37. E. FAWCETT, *Advan. Phys.* **13**, 139 (1964).
38. J. M. ZIMAN, *Phil. Mag.* **3**, 1117 (1958).
39. D. K. C. MACDONALD, W. B. PEARSON, AND I. M. TEMPLETON, *Proc. Roy. Soc. A* **248**, 107 (1958).
40. R. L. POWELL, J. L. HARDEN, AND E. F. GIBSON, *J. Appl. Phys.* **31**, 1221 (1960).